PCCP

ROYAL SOCIETY OF CHEMISTRY

PAPER

View Article Online
View Journal | View Issue

Check for updates

Cite this: *Phys. Chem. Chem. Phys.*, 2024, **26**, 23136

Selective conversion of methane to methanol facilitated by molecular metal–methoxy complexes *via* a self-correcting chemical cycle†

Shahriar N. Khan,‡ Brody Quebedeaux§ and Evangelos Miliordos *

The controlled oxidation of methane to methanol has been an area of intense research over the past decades. Despite the efforts, the identification of an efficient catalyst with high selectivity is still elusive. Here we propose a thoroughly different strategy employing catalysts containing a metal methoxy unit. This family of catalysts has been used for the activation of C–H bonds but this is the first systematic investigation for the conversion of methane to methanol highlighting the advantages over the typically used metal oxides. Specifically, we start our investigation with an Fe(III) center coordinated by four ammonia ligands, $(NH_3)_4FeOCH_3^{2+}$. Structures and energetics are reported for two mechanisms ([2+2] and proton coupled electrons transfer) and for different spin multiplicities *via* density functional theory, multi-reference, and coupled cluster quantum chemical calculations. The excited low-spin doublet state of this model system exhibits the best performance in terms of activation barriers and selectivity. Therefore, we then switched to the corresponding Ru(III) complex, which has a doublet ground state and manifests better performance than the doublet state of Fe(III). For both systems the activation barrier for methanol is larger than that of methane due to the interaction of the OH group of methanol with the coordinated NH_3 ligands (hydrogen bonding) and/or the metal center. This observation suggests that the activation of methanol is slower, hindering its oxidation. In addition, we show that the metal–methoxy family of catalysts offers a potential mechanism that can prevent the oxidation of an activated methanol molecule (self-correcting chemical loop). This work aspires to induce experimental interest and pave the road for the development of high-performance high-selectivity methane to methanol direct conversion routes under mild conditions.

Received 27th May 2024,
Accepted 13th August 2024

DOI: 10.1039/d4cp02189d

rsc.li/pccp

I. Introduction

A financially viable and industrially practical chemical process that can only partially oxidize methane to methanol will render methane a major hydrocarbon feedstock and will reduce the quantities of methane or carbon dioxide released in the atmosphere (methane is a more potent greenhouse gas and thus methane extracted from oil wells is flared).[1] Methanol is a valuable solvent and fuel, it is liquid and thus more easily transported, and it serves as a raw material for the synthesis of larger organic molecules (see ref. 1 and references therein). Ideally, the partial oxidation of methane must occur at the location of the methane extraction, in a single reaction step and under mild conditions. Despite the intense efforts over the past decades from both the experimental and computational fronts, such a chemical process has not been realized yet.

To this end, a variety of homogeneous and heterogeneous systems with metal oxygen bonds have been primarily probed with no satisfactory performance. The methane conversion and methanol selectivity have been proven to be two inversely proportional quantities due to the fact that the C–H bond of methanol is weaker than that of methane.[2,3] The mechanisms, drawbacks, and prospects of these species have been recently reviewed by the authors.[1] Given the limited progress achieved experimentally, there is a big opportunity for quantum chemical calculations to provide guidance. Based on computational results, the authors proposed two main escape exits from this dead-end. First, the produced methanol must be removed fast from the metal center by weakening the interaction between the metal center and methanol. For this purpose, the use of metal oxide anionic units has been suggested.[4,5] An alternative strategy has been recently applied for positively

---

Department of Chemistry and Biochemistry, Auburn University, Auburn, Alabama 36849-5312, USA. E-mail: emiliord@auburn.edu

† Electronic supplementary information (ESI) available. See DOI: **https://doi.org/10.1039/d4cp02189d**

‡ Current address: School of Chemistry and Biochemistry, Georgia Institute of Technology, Atlanta, Georgia 30332-0400, USA.

§ Current address: Department of Chemistry, University of Tennessee, Knoxville, Tennessee 37996-1600, USA.

charged iron catalysts, where the ligands create a hydrophobic environment for the produced methanol.[6] Second, the oxidation reaction of methanol must be slowed down by distorting the corresponding transition state and rendering the activation barrier for methanol higher than that of methane. This can be achieved by employing hydrophilic ligands, which supply hydrogen bond donors.[1,7]

Presently, we provide a third strategy by studying quantum mechanically the reaction of methane and methanol with molecular complexes bearing a metal–methoxy or a metal–methyl unit, which are intermediates of the same catalytic cycle. Tetracoordinated iron(III) and ruthenium(III) ammonia complexes, $[(NH_3)_4MOCH_3]^{2+}$ where M = Fe or Ru, are shown to be superior for two reasons. First, the activation reaction barriers for methanol are higher than methane, and second, the activation of methanol does not necessarily lead to its oxidation, but the produced intermediate can follow a "self-correction" path that returns to the main catalytic cycle. It should also be mentioned that the original form of the catalyst can be $(NH_3)_4MCH_3{}^{2+}$ and form $(NH_3)_4MOCH_3{}^{2+}$ *in situ* (see below). The former species are generally more stable and easier to synthesize.[8]

A very similar Fe(III) molecular complex, $(PY5)FeOCH_3{}^{2+}$ (in which iron is coordinated by five pyridine-type ligands), has been synthesized and its C–H activation ability was probed for various organic molecules (but not methane) producing methanol and organic radicals.[9] The coordination number of the presently studied Fe(III) and Ru(III) differ from $(PY5)FeOCH_3{}^{2+}$ (tetra- *vs.* penta-coordinated complexes). We show below that this is important since it allows the coordination of methane or methanol to the metal improving the performance of the catalyst. Similar observations have been reported in the literature for low-coordination complexes.[10,11] Finally, metal–methoxy moieties (MOMe) have also been suggested as intermediates structures for the activation of methane on metal oxide surfaces,[12] metal–organic frameworks,[13] and zeolites.[14]

To our knowledge, the first study where methane-to-methanol conversion was attempted with metal–methoxy units was carried out by Najafian and Cundari.[15,16] These authors reported complete catalytic cycles for a series of unsaturated (tri-coordinated) complexes scanning over the first row transition metals. More recently, the present authors (S. N. K. and E. M.) employed bare $FeOCH_3{}^{+}$ for the same reaction.[17] However, herein, we employed a ligated $FeOCH_3{}^{2+}$ and its second-row transition metal counterpart $RuOCH_3{}^{2+}$. We show that the dicationic species, and especially the Ru complex, are more efficient in converting methane to methanol due to the adoption of a low spin ground state. The same low-spin state for the Fe complex is generally equally efficient but it is not the ground state.

For the employed dicationic species, $(NH_3)_4FeOCH_3{}^{2+}$ and $(NH_3)_4RuOCH_3{}^{2+}$, we include the activation paths for both methane and methanol. Our work reveals a completely different strategy for the selective formation of methanol introducing a new family of catalysts. This work aspires to serve as a proof-of-concept study and suggests strategies for further improvement of the catalytic performance. Ammonia ligands have been chosen as model ligands with low-computational cost and complexity. Tetradentate ligands, such as triethylenetetraamine or modified derivatives, will be a more realistic option.

II. Computational methods

The geometry optimizations of all intermediate and transition state structures were carried out with density functional theory calculations. The MN15 functional[18] and the cc-pVTZ(C,H,N,Fe) cc-pVTZ-PP(Ru) aug-cc-pVTZ(O) basis sets were chosen.[19–22] The selected functional has shown very good agreement with coupled cluster energetics for the reaction of the very similar $FeOCH_3{}^{+}$ species with methane.[17] The series of diffuse functions on oxygen (aug-) is necessary to describe its O^{-} or O^{2-} character more accurately, and the pseudopotential (PP) for Ru is employed to consider more fully the important scalar relativistic effects for a second-row transition metal atom. For selected key reaction steps, we also performed single point CCSD(T) energy calculations (at the MN15 geometries) with the corresponding double-ζ basis sets. For these cases, the MN15 and CCSD(T) energetics are in very good agreement primarily due to the high single-reference character of the wavefunction (and thus minimal spin-contamination) for the corresponding species as indicated by exploratory CASSCF calculations (see Tables S4 and S5 of the ESI† for the results and technical details). The spin contamination for the ruthenium species is always less than 0.1 (except for one structure). The spin contamination for the sextet states of the iron species is also less than 0.1, for the ground state quartet species it is less than 0.2, while for the higher energy doublet state it ranges from 0.02 to 0.4. For the Ru species we also considered spin–orbit effects, which turned out to correct the energies by less than 1.0 kcal mol^{-1} with the exception of three structures for which the correction is up to 1.7 kcal mol^{-1} (see Table S5 for the numerical results and technical details, ESI†). These corrections nearly cancel each other, with minimal effect on the energy landscape.

All intermediate structures have only real harmonic vibrational frequencies and the transition states have only one imaginary harmonic vibrational frequency. The Cartesian coordinates and frequencies are listed in the ESI.† The reactants and products corresponding to each transition state were confirmed with intrinsic reaction coordinate (IRC) calculations. Free energies for the key reaction steps were estimated using the harmonic approximation at room temperature (20 °C) and atmospheric pressure (1.0 atm). The Gaussian16 software package was invoked for all calculations.[23] Unless explicitly stated, all reported energies are electronic energies. Finally, to bypass several SCF (self-consistent-field) convergence issues we enabled the following options in Gaussian16: "stable = opt" and "scf = (maxcycle = 1000, qc)".

III. Results and discussion

The ideal proposed catalytic cycle for a metal–methoxy dicationic complex $[M]OCH_3{}^{2+}$ ([M] indicates a ligated metal center) is

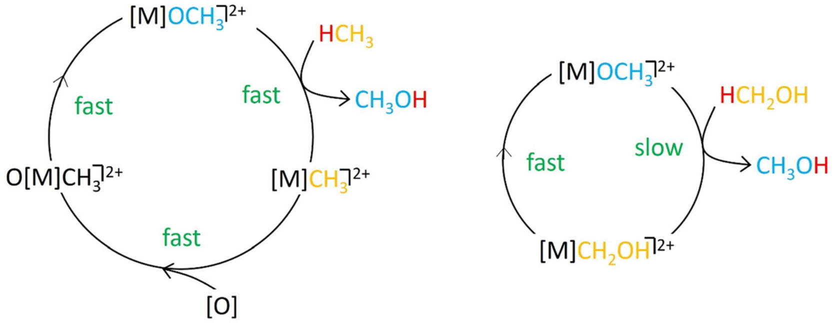

Fig. 1 Proposed catalytic cycles for the conversion of methane to methanol facilitated by metal–methoxy units (left) and for the reaction of methanol with metal–methoxy units (right). The 2+ charge belongs to the whole molecule. The fast/slow comments pertain to the ideal case.

shown in Fig. 1. Similarly to metal oxide dications,[1] the incoming methane can react with the catalyst with either a [2+2] or a radical (proton coupled electron transfer/PCET) mechanism. Depending on the mechanism (see below), the incoming methane provides a hydrogen atom or proton, which joins the methoxy unit to make methanol. In the preferable [2+2] mechanism, the remaining methyl attaches to the metal. The radical mechanism leads to the release of methyl radicals and should be avoided. Then, an oxidant (denoted as [O]) creates a metal–oxo bond, and the resulting complex must isomerize fast to the active form of the catalyst, [M]OCH$_3$$^{2+}$. If the metal–oxo unit survives long enough, it can oxidize methane to methanol as well, but with low selectivity (methane over-oxidation; see ref. 1). As shown below, this unimolecular isomerization step has small activation barriers for dications as opposed to cations; see below and ref. 17. In addition, the [2+2] mechanism is dominant for the low-spin states of the [M] = (NH$_3$)$_4$Fe (excited doublet state) and [M] = (NH$_3$)$_4$Ru (ground doublet state) species.

The main advantage of the proposed family of catalysts lies in their reaction with methanol. As happens for methane, methanol provides a hydrogen atom to produce another methanol molecule, while the remaining CH$_2$OH moiety binds to the metal. This step should ideally be slow, and as shown below it can be slower than methane activation due to the interaction of the hydroxyl group of methanol with either the ammonia ligands (hydrogen bonds) or the metal center. In addition, the formed [M]CH$_2$OH^{2+} species is an isomer of the active form of the catalyst, and it should ideally isomerize fast to [M]OCH$_3$$^{2+}$.

Focusing on the case of [M] = (NH$_3$)$_4$Fe, structures and energetics for the different steps and mechanisms are shown in Fig. 2 and 3. Exact values for the reported energy diagrams are given in the ESI.† Fig. 2 shows all the structures of intermediates and transition states. The catalyst has a trigonal pyramidal conformation with OCH$_3$ occupying one of the axial positions (structure (1)). Methane coordinates weakly to the metal changing the conformation of the complex to pseudo-octahedral (structure (2)). Methane can then be activated either *via* a [2+2] (TS$_{2-3}$) or a radical mechanism (TS$_{2-6}$). Both paths produce methanol, but while the radical mechanism releases a methyl radical (structure (6)), the [2+2] path keeps CH$_3$ coordinated to iron (structure (3)). For all spin multiplicities, the radical path is unfavorable since the reverse reaction is exothermic and has lower reverse activation barriers (see Fig. 3).

The 3d^5 electrons of the Fe^{3+} center can couple into a doublet, quartet, or sextet spin state. The sextet state of (NH$_3$)$_4$FeOCH$_3$$^{2+}$ is the ground state and can follow only a radical mechanism. The quartet state (just 1.5 kcal mol^{-1} higher) follows both pathways with the radical transition state (TS$_{2-6}$) being 11.0/18.5 kcal mol^{-1} (electronic/free energy) more stable than [2+2] (TS$_{2-3}$). Interestingly, the situation is reversed in the doublet state of (NH$_3$)$_4$FeOCH$_3$$^{2+}$ (11.7 kcal mol^{-1} higher than $S = \frac{5}{2}$), where TS$_{2-3}$ is lower than TS$_{2-6}$ by 5.2 kcal mol^{-1} (electronic energy) or slightly higher by 2.2 kcal mol^{-1} (free energy). The activation free energy barriers are relatively large in every case ranging between 17.3 (TS$_{2-6}$ for $S = \frac{3}{2}$) and 35.3 (TS$_{2-3}$ for $S = \frac{3}{2}$) kcal mol^{-1}.

The radical mechanism proceeds as proton coupled electron transfer (PCET). One proton from methane is captured from a lone pair of oxygen making the OH bond, and one electron moves from methane to Fe^{3+}, and specifically its 3d$_{z^2}$ orbital. The orbitals before and after PCET for $S = \frac{3}{2}$ are shown in Fig. S1 (ESI†) confirming this process. The [2+2] mechanism cleaves the activated C–H bond heterolytically shuttling one proton to oxygen and the CH$_3$$^{-}$ moiety to iron. Both mechanisms follow closely the mechanism observed in the methane activation facilitated by metal oxides.[1] For metal oxides, the [2+2] path bears generally larger activation barriers and the same is observed here for the quartet and sextet states.

The doublet state of the present system is a counter-example and imitates the doublet state of the (NH$_3$)$_4$RhO^{2+} complex.[7] The two systems are isovalent bearing a d^5 metal center: [(NH$_3$)$_4$(Fe^{3+})(OCH$_3$$^{-}$)]$^{2+}$ *vs.* [(NH$_3$)$_4$(Rh^{4+})(O^{2-})]$^{2+}$. The very low activation barrier of the Rh complex (13.6 kcal mol^{-1}) was attributed to the electronic structure change upon the complexation of methane.[1,7] The d^5 electrons adopted a t$_{2g}^5$ configuration which exposed the Rh^{4+} charge to the CH bond electrons pre-activating methane. The present iron complex has a more complex electronic structure mixing a t$_{2g}^5$ and a t$_{2g}^4$e$_g^1$ as suggested by the natural orbitals shown in Fig. 4, which results in a higher activation barrier (22.8 kcal mol^{-1}). Finally, methanol release requires 26.0 ($S = \frac{3}{2}$) and 38.4 ($S = \frac{1}{2}$) kcal mol^{-1} energies,

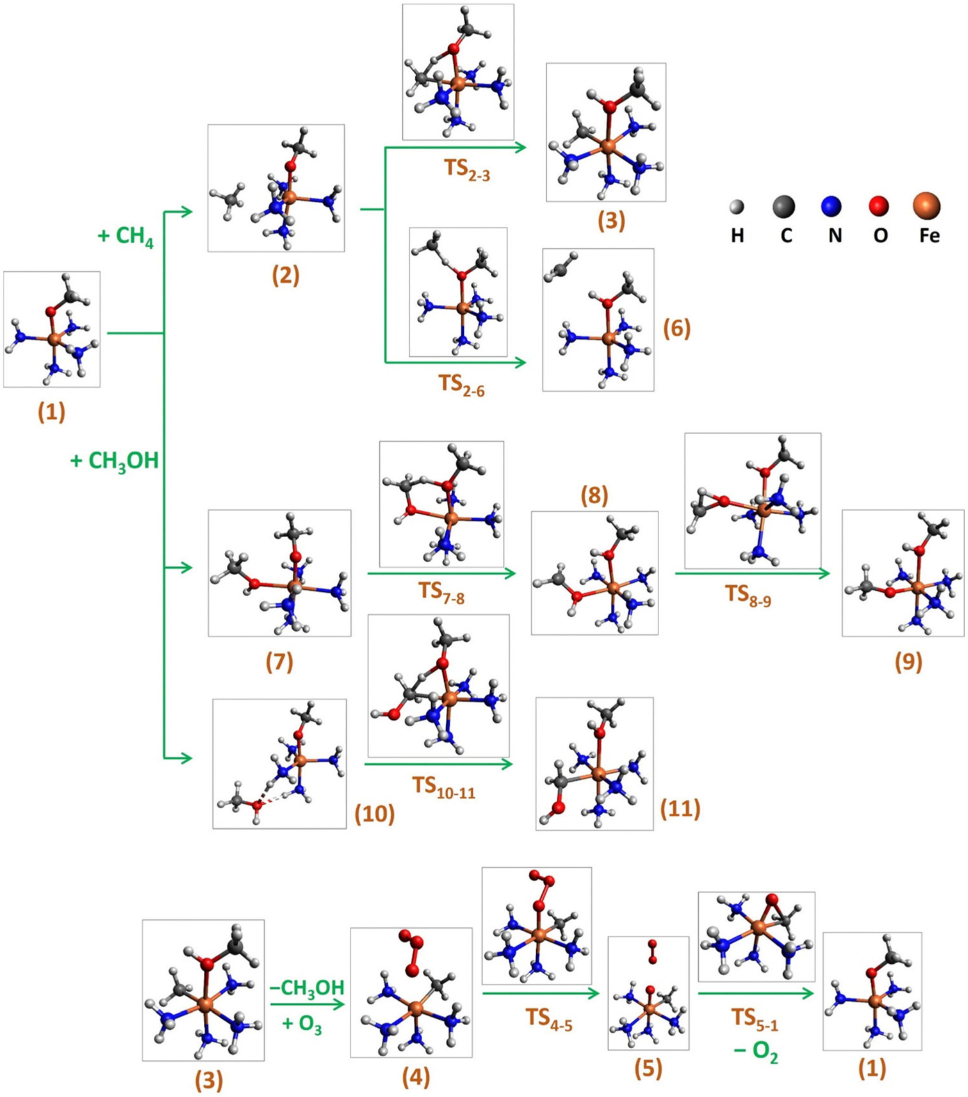

Fig. 2 Optimized structures pertaining to the catalytic cycles in Fig. 1 for the quartet spin state of [M] = $(NH_3)_4Fe$ and [O] = O_3.

which drop to 12.8 and 23.3 kcal mol^{-1} (free energies), respectively, due to the entropy increase.

The activation of methanol happens with the same two mechanisms. The PCET path goes *via* structures (7) and TS$_{7–8}$, while [2+2] *via* (10) and TS$_{10–11}$. The main difference between the methanol from methane structures is the interactions of the OH group with either the ammonia ligands (hydrogen bonding) or with the metal center (coordinative/dative bonding). Hydrogen bonding was suggested recently as a means to perturb the transition state of methanol and increase the activation barrier.[7] Similar strategies have been used for the activation of specific C–H bonds of larger organic molecules.[24,25] Currently, we observe that the metal–oxygen coordination can play the same role. The calculated free energy activation barriers range from 22.1 (radical, $S = \frac{3}{2}$) to 43.1 ([2+2], $S = \frac{3}{2}$) kcal mol^{-1}, and are consistently higher than those of methane by at least 4.8 kcal mol^{-1} ([2+2], $S = \frac{1}{2}$) and up to 7.9 ([2+2], $S = \frac{3}{2}$) kcal mol^{-1}, which increases the selectivity towards methanol production.[7]

The PCET/[2+2] pathways generate the structures (8)/(11), both of which can isomerize to $(NH_3)_4FeOCH_3{}^{2+}$ after they release methanol. In structure (8), the produced CH_2OH has a smaller dissociation energy than methanol and the isomerization to structure (9) should occur before the methanol release. The located TS$_{8–9}$ structure is 34.3–36.2 kcal mol^{-1} (free energy, depending on the spin state; see Fig. 5) higher than (8), which makes the proposed isomerization path of the right cycle of Fig. 1 very slow. The reaction is exothermic (structure (9) is lower than (8); see Fig. 5) and we believe that our future explorations in a larger chemical space will disclose appropriate metal–ligands combinations. We were not able to identify the mechanism going from structures (11) to (9) for iron, but we did for ruthenium for which the activation barriers are also high (see below).

Given that the excited doublet state of $(NH_3)_4FeOCH_3{}^{2+}$ has competitive [2+2] and PCET free energy activation barriers, we examined its second-row transition metal analogue

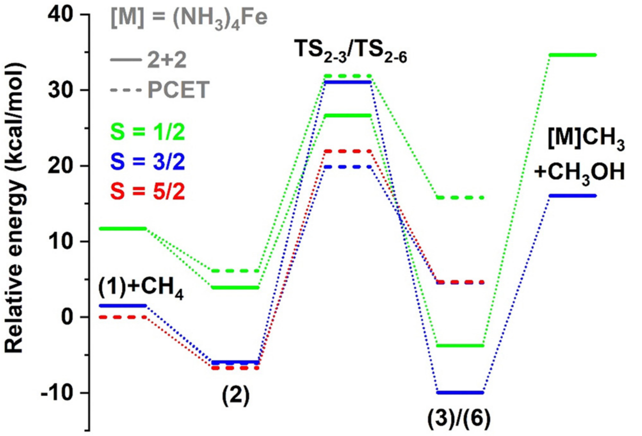

Fig. 3 MN15 electronic energy diagrams for the $(NH_3)_4FeOCH_3^{2+}$ + CH_4 reaction in the doublet (green), quartet (blue), and sextet (red) spin multiplicity potential energy profiles. The *X*/*Y* or (*X*)/(*Y*) notation, *i.e.* (3)/(6), corresponds to [2+2]/PCET reaction paths.

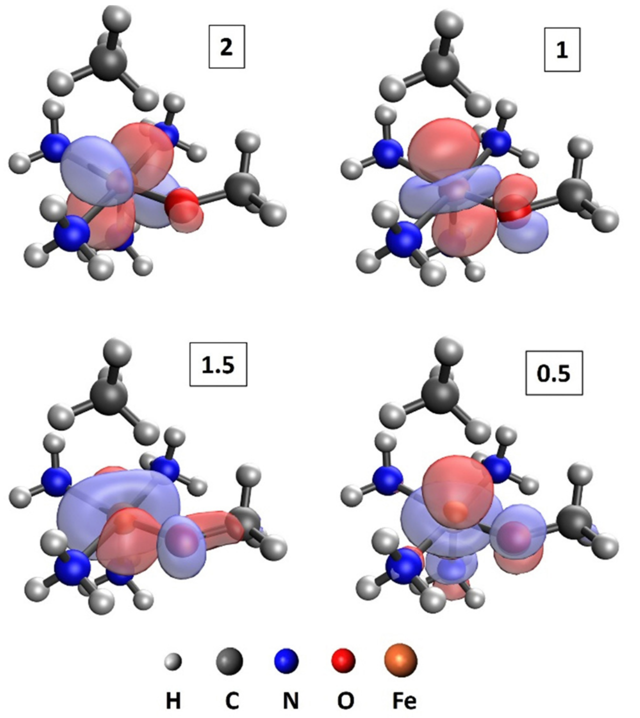

Fig. 4 MN15 natural orbitals of the $(NH_3)_4(CH_4)FeOCH_3^{2+}$ complex ($S = \frac{3}{2}$). The numbers in the boxes pertain to the occupancy of each orbital.

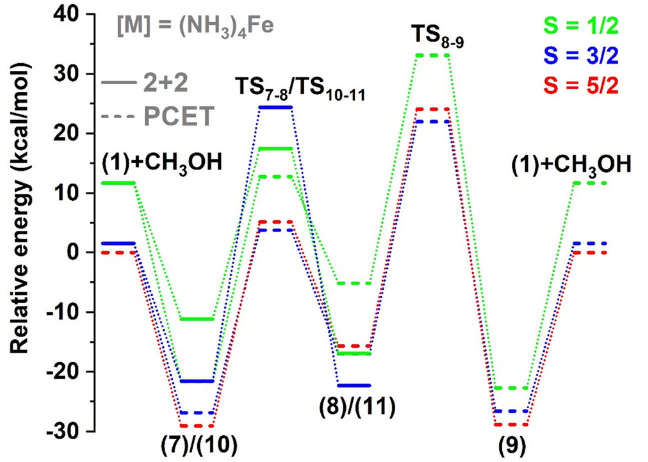

Fig. 5 MN15 electronic energy diagrams for the $(NH_3)_4FeOCH_3^{2+}$ + CH_3OH reaction in the doublet (green), quartet (blue), and sextet (red) spin multiplicity potential energy profiles. The *X*/*Y* or (*X*)/(*Y*) notation corresponds to PCET/[2+2] reaction paths.

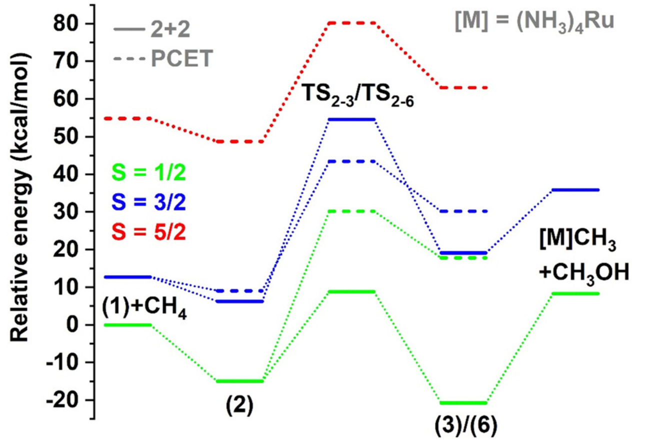

Fig. 6 MN15 electronic energy diagrams for the $(NH_3)_4RuOCH_3^{2+}$ + CH_4 reaction in the doublet (green), quartet (blue), and sextet (red) spin multiplicity potential energy profiles. The *X*/*Y* or (*X*)/(*Y*) notation corresponds to [2+2]/PCET reaction paths.

$(NH_3)_4RuOCH_3^{2+}$, which is expected to have a low spin ground state. For example, FeO^{2+} has a triplet ground state with two nearly degenerate high spin (quintet/septet) states, while the ground state of RuO^{2+} is singlet and well separated from the first excited state (triplet).[26,27] Indeed, the ground state of $(NH_3)_4RuOCH_3^{2+}$ was found to be the doublet state (well separated from the quartet and sextet; see Fig. 6) with superior performance. The production of methanol from the reaction of a ruthenium methoxy unit and phenol in a similar mechanism to that currently proposed has been reported experimentally.[28]

Compared to iron, the OCH_3 unit occupies one of the equatorial positions of the $(NH_3)_4RuOCH_3^{2+}$ complex. The [2+2] activation barrier is now appreciably smaller than the PCET one ($\Delta G^\ddagger$ = 21.6 *vs.* 39.2 kcal mol^{-1}), while the reverse PCET reaction step is even more favorable avoiding completely the production of CH_3 radical. In addition, the methanol activation is clearly slower ($\Delta G^\ddagger$ = 25.4 kcal mol^{-1} for [2+2]; see Table 1 and Fig. 7). To see if these three values are artifacts of DFT, we did CCSD(T) calculations with the corresponding double-ζ basis sets and we obtained electronic energy barriers of 23.3, 42.4, and 28.5 kcal mol^{-1}, which compare favorably to the 23.7 (corresponding to $\Delta G^\ddagger$ = 21.6), 45.1 (corresponding to $\Delta G^\ddagger$ = 39.2), and 28.7 (corresponding to $\Delta G^\ddagger$ = 25.4) kcal mol^{-1}

Table 1 Forward (ΔG_{forw}) and reverse (ΔG_{revs}) activation free energy values (in kcal mol^{-1}) for the reaction steps of Fig. 2 pertaining to [M] = $(NH_3)_4Fe$ and $(NH_3)_4Ru$

	ΔG_{forw}					ΔG_{revs}				
	[M] = $(NH_3)_4Fe$			[M] = $(NH_3)_4Ru$		[M] = $(NH_3)_4Fe$			[M] = $(NH_3)_4Ru$	
	$S = \frac{1}{2}$	$S = \frac{3}{2}$	$S = \frac{5}{2}$	$S = \frac{1}{2}$	$S = \frac{3}{2}$	$S = \frac{1}{2}$	$S = \frac{3}{2}$	$S = \frac{5}{2}$	$S = \frac{1}{2}$	$S = \frac{3}{2}$
ΔG_{2-3}	23.6	35.3		21.6	46.3	28.2	38.9		28.1	32.8
ΔG_{4-5}[a]		4.9	0.2	−0.3	−0.5		11.2	20.6	32.7	41.8
ΔG_{5-1}	0.6	1.9	6.9	17.4	14.4	64.4	67.3	84.4	42.3	47.1
ΔG_{2-6}	21.0	17.3	23.0	39.2	30.7	15.8	15.6	16.8	11.6	13.0
ΔG_{7-8}	26.6	22.1	30.0	36.8	30.6	17.3	19.9	20.5	13.8	14.7
ΔG_{8-9}	34.3	35.7	36.2	35.0	30.0	45.2	38.7	47.0	59.1	30.5
ΔG_{10-11}	28.4	43.1		25.4		33.1	45.9		32.8	

[a] For $[Ru]CH_3^{2+} + N_2O \leftrightarrow O[Ru]CH_3^{2+} + N_2$: ΔG_{forw} = 22.4 kcal mol^{-1} and ΔG_{revs} = 52.0 kcal mol^{-1}.

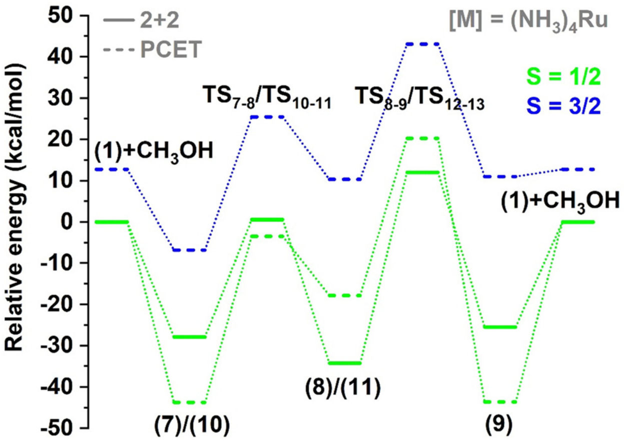

Fig. 7 MN15 electronic energy diagrams for the $(NH_3)_4RuOCH_3^{2+}$ + CH_3OH reaction in the doublet (green), quartet (blue), and sextet (red) spin multiplicity potential energy profiles. The *X*/*Y* or (*X*)/(*Y*) notation corresponds to PCET/[2+2] reaction paths.

values of MN15. Overall, the activation of methane is considerably faster and the production of CH_3 radicals is very unlikely. At the same time, the methanol release free energy is 15.8 kcal mol^{-1} (*vs.* 23.3 for $S = \frac{1}{2}$ of $(NH_3)_4FeOCH_3^{2+}$), which makes the removal of methanol by the solvent easier, increasing the selectivity towards methanol.[2]

A striking difference between $(NH_3)_4FeOCH_3^{2+}$ and $(NH_3)_4RuOCH_3^{2+}$ is the coordination mode of methane to Ru. For all spin states and for both metals, except for the doublet state of $(NH_3)_4RuOCH_3^{2+}$, methane coordinates weakly at a distance of at least 3.3 Å. In the doublet state of $(NH_3)_4RuOCH_3^{2+}$, methane approaches the Ru center to 2.6 Å and one of the C–H bonds elongates by 0.03 Å compared to free CH_4 (from 1.087 to 1.119 Å). The same effect takes place when CH_4 approaches the ground doublet state of $(NH_3)_4RhO^{2+}$.[7] The metal centers in both cases have a pure t_{2g}^5 electronic configuration, which exposes the electrons of the activated C–H bond to the formally +3 (Ru) or +4 (Rh) metallic charges.[7] The larger charge of Rh causes a bigger elongation of the C–H bond (0.04 Å).[7]

As in $(NH_3)_4FeOCH_3^{2+}$, the loop mechanism converting structures (8) or (11) to (9) (see the right cycle of Fig. 1) is hindered by large barriers. The (8)-to-(9) and (11)-to-(9) barriers are 38.1 and 46.2 kcal mol^{-1}, respectively. The TS_{8-9} structure is like that of iron (see Fig. 2), but the conversion of (11) to (9) requires the release of methanol first (structure (12) in Fig. S2 of the ESI†). The whole mechanism and the corresponding energy diagram are shown in Fig. S2 and S3 of the ESI.† Fig. 7 shows only the energy of the TS_{12-13} transition state pertaining to the rate determining step.

The last part of our discussion pertains to the oxidation of the catalyst and closure of the cycle. Here we used O_3, which anchors to $[M]CH_3^{2+}$ (structure (4) of Fig. 2) oxidizing it to $O[M]CH_3^{2+}$ and releasing molecular oxygen (O_2) after TS_{4-5}. The metal oxide of structure (5) finally isomerizes to structure (1) *via* TS_{5-1} closing the catalytic cycle. For M = Ru, we also considered N_2O as the oxidant. Both O_3 and N_2O are closed-shell singlet molecules, but the ejected O_2 and N_2 after the donation of one oxygen atom are of different spin multiplicity (triplet for O_2 and closed-shell singlet for N_2). Therefore, the spin multiplicity of $O[M]CH_3^{2+}$ remains the same as in $[M]CH_3^{2+}$ for N_2O but may change for O_3. It turns out that even for O_3 the spin multiplicity is preserved. Specifically, the ground state of $O[Fe]CH_3^{2+}$ has $S = \frac{3}{2}$, which combined with S = 1 of O_2 generates $S = \frac{1}{2}, \frac{3}{2}, \frac{5}{2}$. Therefore, all spin $[M]CH_3^{2+} + O_3$ states will go to $O[Fe]CH_3^{2+}$ ($S = \frac{3}{2}$) + O_2 (S = 1), which finally leads to the ground state of $[Fe]OCH_3^{2+}$ ($S = \frac{3}{2}$). Next, the ground state of $O[Ru]CH_3^{2+}$ is doublet ($S = \frac{1}{2}$), which correlates to $S = \frac{1}{2}$ and $S = \frac{3}{2}$ of $O[Ru]CH_3^{2+}$ + O_2. Thus, both $S = \frac{1}{2}$ and $S = \frac{3}{2}$ of $[Ru]CH_3^{2+} + O_3$ go to $O[Ru]CH_3^{2+}$ ($S = \frac{1}{2}$) which leads to the ground state $S = \frac{1}{2}$ of $[Ru]OCH_3^{2+}$. Fig. 8 collects the energetics for all three spins of the $[Fe]CH_3^{2+} + O_3$ reaction pathways, for $S = \frac{1}{2}$ and $\frac{3}{2}$ of $[Ru]CH_3^{2+} + O_3$, and for $S = \frac{1}{2}$ of $[Ru]CH_3^{2+} + N_2O$. The sextet state of the Ru complex is very high in energy (see above) and is not considered here.

Energetically, the oxidation step is practically barrier-free for O_3 for all iron species with barriers of less than 5.0 kcal mol^{-1}. The reaction of $[Ru]CH_3^{2+}$ with O_3 is also barrier-free but has a barrier of 22.4 kcal mol^{-1} with N_2O (see Table 1). N_2O was found to be more effective for electron-rich metal centers.[4,5] The products in both cases are equally stable with respect to the reactants by 33.0 kcal mol^{-1}. Overall, the choice of an oxidant can affect the oxidation rate and the performance of the catalyst. Ideally, molecular oxygen must be used and will be a

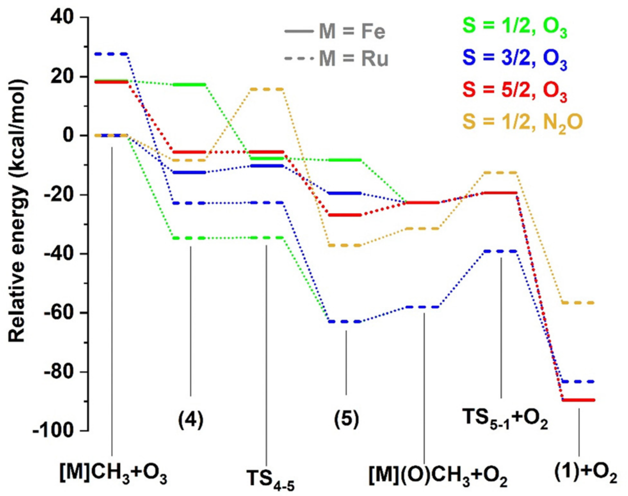

Fig. 8 MN15 electronic energy diagrams for the $(NH_3)_4MCH_3^{2+}$ + O_3 or N_2O reaction in the doublet (green), quartet (blue), and sextet (red) spin multiplicity potential energy profiles. Single point energy calculations at the geometries of the quartet state are performed for the doublet state of M = Fe.

topic of future studies. A considerably more complex mechanism is expected, which is out of our scope. The isomerization step is practically spontaneous ($\Delta G^{\ddagger} \leq 7.0$ kcal mol^{-1}; see Table 1) for iron but has a barrier of $\Delta G^{\ddagger} = 17.4$ kcal mol^{-1} for ruthenium.

A final comment pertains to the β-hydrogen elimination. The $(NH_3)_4RuOCH_3^{2+}$ form of the catalyst can undergo a hydride transfer from carbon to ruthenium forming $(NH_3)_4RuH(OCH_2)^{2+}$, which degrades the catalyst and can release formaldehyde (CH_2O); see for example ref. 29 for the same reaction step in a palladium complex. The two species, $(NH_3)_4RuOCH_3^{2+}$ and $(NH_3)_4RuH(OCH_2)^{2+}$, are practically isoenergetic with the latter being only 0.7 and 0.4 kcal mol^{-1} lower in energy at MN15 and CCSD(T) levels, respectively (see Fig. S4 and S5 of the ESI† for structures and energetics). The free energy favors the former by 0.1 kcal mol^{-1}, the two species are separated by minimal energy barriers of less than 0.6 kcal mol^{-1} (CCSD(T)), and the release of CH_2O is highly endothermic ($\Delta G = 30.6$ kcal mol^{-1}). These results suggest that there is a fast equilibrium between the two stable $(NH_3)_4RuOCH_3^{2+}$ and $(NH_3)_4RuH(OCH_2)^{2+}$ isomers. The consumption of $(NH_3)_4RuOCH_3^{2+}$ *via* the catalytic cycle of Fig. 1 will shift the equilibrium avoiding the β-hydrogen elimination reaction.

IV. Conclusions and outlook

In summary, we carried out quantum chemical calculations to study the performance of metal–methoxy or metal–methyl species for the selective conversion of methane to methanol. These systems have been employed in the literature in both experimental and theoretical studies for the activation of hydrocarbons, but no systematic work has appeared in the literature for the conversion of methane to methanol. Here we focused on $(NH_3)_4FeOCH_3^{2+}$/$(NH_3)_4FeCH_3^{2+}$ and $(NH_3)_4RuOCH_3^{2+}$/$(NH_3)_4RuCH_3^{2+}$ to demonstrate the superior potential (especially of the latter species) over the commonly used metal oxide complexes. This novel strategy offers the following advantages:

(1) The radical mechanism is completely suppressed, *i.e.* no production of CH_3 radicals is expected.

(2) The activation barriers for methane *via* the preferred [2+2] mechanism are reasonable.

(3) The activation barriers for methanol are higher than that of methane resulting to slower oxidation of methanol and higher selectivity towards methanol. The higher barrier for methanol is attributed to the distortion of the pertinent transition state caused by the formation of hydrogen bonding or the coordination of methanol to the metal.

(4) Even if methanol is activated, the produced intermediates, $(NH_3)_4MOHCH_2^{2+}$ or $(NH_3)_4MCH_2OH^{2+}$, can in principle loop back to the original form of the catalyst, $(NH_3)_4MOCH_3^{2+}$, avoiding completely the oxidation of methanol.

(5) The oxidation of the metal center with O_3 (in contrast with N_2O) is facile.

(6) The oxidation of the metal center leads to $(NH_3)_4M(O)CH_3^{2+}$ which isomerizes to the desirable $(NH_3)_4MOCH_3^{2+}$ structure with low activation barriers, avoiding the oxidation of methane from the metal–oxo bond.

We showed that the excited doublet state of Fe(III) has better features than the ground quartet state. Switching to the second-row analog Ru(III) we were able to stabilize the doublet state, which is now the ground state and bears even better features than the doublet state of Fe(III). For better exploitation of the presently proposed family of catalysts, more work is needed to identify molecular complexes with lower $[M]OHCH_2^{2+}/[M]CH_2OH^{2+} \rightarrow [M]OCH_3^{2+}$ isomerization barriers which also prevent elimination of the β-hydrogen in $[M]OCH_3^{2+}$. To this direction, the exploration of the vast chemical space along dimensions such as metal identity, ligand effects, solvent contributions, oxidation states, and synergistic chemistry is underway. Machine learning techniques have been used for such explorations regarding direct methane to methanol conversion.[30] Finally, O_2 should be considered as an oxidant in future studies.

In terms of electronic structure, our present and older studies,[1,7] indicate that the metal should bear an electronic structure that facilitates the approach of methane close to the positively charged metal center, and this is achieved more easily with low-spin states. Therefore, second row transition metals are more advantageous. However, the use of the more abundant first-row metals combining them with appropriate ligands will be a more cost-effective route. This work serves as a communication for the importance of the titled species and the exploration of a larger region of the chemical space is in progress.

Data availability

All data that support the findings of this study are included within the article. The numerical values used for the production of the figures are given in the ESI.† The software used for the generation of the data is cited in the references.

Conflicts of interest

There are no conflicts to declare.

Acknowledgements

E. M. is indebted to Auburn University for financial support and especially the James E. Land endowment. This work was completed with resources provided by the Auburn University Easley Cluster.

References

1 E. E. Claveau, S. Sader, B. A. Jackson, S. N. Khan and E. Miliordos, *Phys. Chem. Chem. Phys.*, 2023, **25**, 5313–5326.
2 A. A. Latimer, A. Kakekhani, A. R. Kulkarni and J. K. Nørskov, *ACS Catal.*, 2018, **8**, 6894–6907.
3 M. Ravi, M. Ranocchiari and J. A. van Bokhoven, *Angew. Chem., Int. Ed.*, 2017, **56**, 16464–16483.
4 S. Sader and E. Miliordos, *J. Phys. Chem. A*, 2021, **125**, 2364–2373.
5 S. Sader and E. Miliordos, *Phys. Chem. Chem. Phys.*, 2022, **24**, 21583–21587.
6 H. Fujisaki, T. Ishizuka, H. Kotani, Y. Shiota, K. Yoshizawa and T. Kojima, *Nature*, 2023, **616**, 476–481.
7 E. E. Claveau, E. R. Heller, J. O. Richardson and E. Miliordos, *J. Phys. Chem. Lett.*, 2023, **14**, 8749–8754.
8 J. Campos, J. López-Serrano, R. Peloso and E. Carmona, *Chem. – Eur. J.*, 2016, **22**, 6432–6457.
9 C. R. Goldsmith, R. T. Jonas and T. D. P. Stack, *J. Am. Chem. Soc.*, 2002, **124**, 83–96.
10 L. J. Taylor and D. L. Kays, *Dalton Trans.*, 2019, **48**, 12365–12381.
11 A. W. Pierpont and T. R. Cundari, *J. Coord. Chem.*, 2011, **64**, 3123–3135.
12 Z. Liu, E. Huang, I. Orozco, W. Liao, R. M. Palomino, N. Rui, T. Duchoň, S. Nemšák, D. C. Grinter and M. Mahapatra, *et al.*, *Science*, 2020, **368**, 513–517.
13 M. C. Simons, S. D. Prinslow, M. Babucci, A. S. Hoffman, J. Hong, J. G. Vitillo, S. R. Bare, B. C. Gates, C. C. Lu and L. Gagliardi, *et al.*, *J. Am. Chem. Soc.*, 2021, **143**, 12165–12174.
14 V. L. Sushkevich, D. Palagin, M. Ranocchiari and J. A. van Bokhoven, *Science*, 2017, **356**, 523–527.
15 A. Najafian and T. R. Cundari, *Inorg. Chem.*, 2017, **56**, 12282–12290.
16 A. Najafian and T. R. Cundari, *Organometallics*, 2018, **37**, 3111–3121.
17 S. N. Khan and E. Miliordos, *J. Phys. Chem. A*, 2019, **123**, 5590–5599.
18 H. S. Yu, X. He, S. L. Li and D. G. Truhlar, *Chem. Sci.*, 2016, **7**, 5032–5051.
19 N. B. Balabanov and K. A. Peterson, *J. Chem. Phys.*, 2005, **123**, 064107.
20 T. H. Dunning, *J. Chem. Phys.*, 1989, **90**, 1007–1023.
21 D. Figgen, K. A. Peterson, M. Dolg and H. Stoll, *J. Chem. Phys.*, 2009, **130**, 164108.
22 R. A. Kendall, T. H. Dunning and R. J. Harrison, *J. Chem. Phys.*, 1992, **96**, 6796–6806.
23 M. J. Frisch, G. W. Trucks, H. B. Schlegel, G. E. Scuseria, M. A. Robb, J. R. Cheeseman, G. Scalmani, V. Barone, G. A. Petersson and H. Nakatsuji, *et al.*, *Gaussian 16 Rev. B.01*, 2016.
24 J. R. Frost, S. M. Huber, S. Breitenlechner, C. Bannwarth and T. Bach, *Angew. Chem., Int. Ed.*, 2015, **54**, 691–695.
25 G. Olivo, G. Farinelli, A. Barbieri, O. Lanzalunga, S. Di Stefano and M. Costas, *Angew. Chem., Int. Ed.*, 2017, **56**, 16347–16351.
26 N. M. S. Almeida, I. R. Ariyarathna and E. Miliordos, *J. Phys. Chem. A*, 2019, **123**, 9336–9344.
27 J. K. Kirkland, S. N. Khan, B. Casale, E. Miliordos and K. D. Vogiatzis, *Phys. Chem. Chem. Phys.*, 2018, **20**, 28786–28795.
28 B. S. Kang, U. Koelle and U. Thewalt, *Organometallics*, 1991, **10**, 2569–2573.
29 L. M. Martínez-Prieto, E. Ávila, P. Palma, E. Álvarez and J. Cámpora, *Chem. – Eur. J.*, 2015, **21**, 9833–9849.
30 A. Nandy, C. Duan, C. Goffinet and H. J. Kulik, *JACS Au*, 2022, **2**, 1200–1213.